Chemical and Process Engineering Research
ISSN 2224-7467 (Paper) ISSN 2225-0913 (Online)
Vol.21, 2014

The Chemical Chelates and a Comparative Antimicrobial Study on Some Ciprofloxacin Complexes, Spectral, Kinetic and Molecular Modeling Investigations

Gamil A.A. Al-Hazmi [1,2*] and Fawaz A. Saad[3]

[1] Chemistry Department, Faculty of Applied Science, Taiz University, P.O. Box 82, Taiz, Yemen
[2]Chemistry Department, Faculty of Science, King Khalid University, P.O. Box 9004, Abha, Saudi Arabia
[3]Chemistry department, Faculty of Applied Science, Umm Al- Qura University, Makkah, Saudi Arabia
* E-mail of the corresponding author: gamilalhazmi@hotmail.com

Abstract
A series of ciproH antibiotic drug complexes was prepared. Cu(II), VO(II), Pd(II), Zn(II), Pt(II) and Pt(IV) are the metal ions used for the preparations. The chosen ions have a great history in the medicinal field which may introduce a sensitive antibiotic appearance in comparing with the free ciproH drug. All the prepared complexes are discussed briefly based on spectral (IR, ^{1}HNMR, ^{13}CNMR, Uv-Vis, ESR, X- ray and SEM), thermal and analytical data. The ligand coordinates through its zwitterionic form as bidentate mod through COO^{-} and C=O groups. The octahedral stereo structure was prepared with Cu(II), Zn(II) and Pt(IV) ions, square planer with Pd(II) and Pt(II) ions however, the square – pyramidal with VO(II) ion. The amorphous nature was proposed for all investigated complexes based on the x- ray diffraction patterns although, the nanocrystalline appearance of starting ligand. Thermogravimetric analysis is also used to support the presence or absence of solvent molecules conjugated with the complexes isolated physically or chemically. Applying Chem- office program a suitable modeling structure of each investigated complex was drawn. A comparative antibacterial study was concerned using Gramm –ve and Gramm +ve bacteria . The data reflect the inhibiting effect of some complexes more than the drug itself which is considered an introductory step in introducing competitive drug.

Key words: ciprofloxacin complexes, spectral, modeling and biological activity

1. Introduction

Several antibiotics interact with a variety of biomolecules, which may result in inhibition of the biochemical or biophysical processes associated with the biomolecules. This can be illustrated in the interaction of the peptide antibiotic polymyxin with glycolipids which affects membrane function [1]. The intercalation of the anthracyclines (ACs) into DNA base pairs which stops gene replication [2] in the imbedding of the lipophilic antibiotic gramicidin [3] and the insertion of the amphiphilic antibiotic protein into cell membrane [4] which disturb normal ion transport and trans-membrane potential of cells, in the inhibition of transpeptidase by penicillin which affects cell wall synthesis [5] and the inhibition of aminopeptidase by bestatin, amastatin, and puromycin which impairs many significant biochemical processes[6,7]. There are several families of antibiotics that require metal ions to function properly [2–7]. In some cases, metal ions are bound tightly and are integral parts of the structure and function of the antibiotics. Removal of the metal ions thus results in deactivation and/or change in structure of these antibiotics, such as bacitracin, bleomycin (BLM), streptonigrin (SN), and albomycin. In other cases, the binding of metal ions to the antibiotic molecules may engender profound chemical and biochemical consequence, which may not significantly affect the structure of the drugs, such as tetracyclines

(TCs), ACs, aureolic acids, and quinolones. When dealing with the interaction between drugs and metal ions in living systems, a particular attention has been paid to the interaction of metal ions with antibiotics. Antibiotics that interact with metal ions constituted a class of drugs which has been widely used in medicine both for human beings and animals [8,9]. In particular, the interaction between transition metals and b-lactamic antibiotics such as cephalexin had been recently investigated by several physicochemical and spectroscopic methods with detailed biological data [10–13]. Many drugs possess modified pharmacological and toxicological properties when administered in the form of metallic complexes. Probably the most widely studied cation in this respect is Cu(II), for which a host of low-molecular-weight Cu(II) complexes have been proved beneficial against several diseases such as tuberculosis, rheumatoid arthritis, gastric ulcers, and cancers [14–17]. There has been a tremendous growth in the study of drugs from quinolone family, which began with the discovery of nalidixic acid some over 40 years ago. Since then, the exponential growth of this family had produced more than ten thousand analogues [18]. Floxacin family is considered the best of the third generation quinolone family. There are several reports regarding the synthesis and crystal structure of metal complexes with quinolone derivatives [19–22]. Quinolone antibiotics could participate in the formation of complexes in number of ways [23–27]. In acidic media, quinolones are usually singly and/or doubly protonated making them unable to coordinate to the metal cations and, in such cases, only electrostatic interaction are observed between the drug and the metal ions [28]. Metalloantibiotics can interact with several different kinds of biomolecules, including DNA, RNA, proteins, receptors, and lipids, rendering their unique and specific bioactivities. In addition to the microbial-originated metalloantibiotics, many metalloantibiotic derivatives and metal complexes of synthetic ligands also show antibacterial, antiviral, and anti-neoplastic activities which are also briefly discussed to provide a broad sense of the term ‘‘metalloantibiotics’’. There are several metal–floxacin complexes and their biological activity studies have been reported [23–28]. This study concerning with the preparation of new series of ciprofloxacin complexes. Elaborated investigation was carried out serving all possible tools. A comparative biological study is a major focus over different bacteria. An interest in this paper is developing a modular form of the effectiveness of antibiotics on the biological effects resulting from the interaction between the metal ions and ciproH antibiotic ligand.

2. Experimental

2.1. General reagents

Ciprofloxacin (Fig.1) used in this study was obtained from the Egyptian International Pharmaceutical Industrial Company (EIPICO). All chemicals used for the preparation of complexes were of analytical reagent grade, commercially available from Fluka. $Cu(NO_3)_2.3H_2O$, $PdCl_2$, $PtCl_2$, $PtCl_4$, $Zn(NO_3)_2.6H_2O$ and $VOSO_4.2.5H_2O$ were used without further purification.

2.2. Synthesis of the complexes

2 mmol of ciproH ligand suspended in 40 ml of ethanol was mixed with 2 mmol of $Cu(NO_3)_2.3H_2O$, $PdCl_2$, $PtCl_2$, $PtCl_4$, $Zn(NO_3)_2.6H_2O$ and $VOSO_4.2.5H_2O$ in 10 ml ethanol solvent. Aqueous potassium chloride was added with $PtCl_2$ and $PdCl_2$ solutions for complete salvation. The reaction medium of VO(II) salt was carried out

in presence of sodium acetate to produce a slightly basic medium to isolate the complex. The reaction mixture was kept at 80- 90 ^{o}C for about 2 – 4 h. The product obtained was collected by filtration and washed with a mixture of ethanol / water (50 : 50). The product thus obtained was dried (90 ^{o}C) and then left under vacuum over anhydrous calcium chloride.

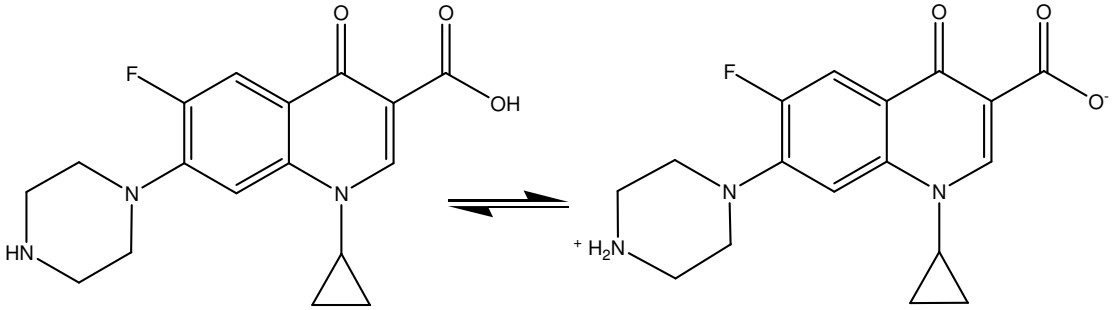

Ciprofloxacin Zwitter ioic structure

Figure 1. Structure of ciprofloxacin and its zwitterionic form.

2.3. Antibacterial Investigation.

The procedure described by Gupta et al. [29] was employed. The investigated isolates of bacteria were seeded in tubes with nutrient broth (NB). The seeded NB (1 mL) was homogenized in the tubes with 9 mL of melted (45 °C) nutrient agar (NA). The homogeneous suspensions were poured into Petri dishes and left until solidified. Some holes were spread on the top of the solidified media. Holes having a diameter of 4 mm were impregnated with 2 X 10^{-3} cm^3 of the test. After incubation for 24 h in a thermostat at 25 °C, the inhibition (sterile) zone diameters (including disk) were measured and expressed in millimeters. An inhibition zone diameter over 7 mm indicates that the tested compound is active against the bacteria under investigation. The antibacterial activities of the investigated compounds were tested against Klebsiella sp. and Proteus sp. (Gram - ve) and Bacillus subtilis (Gram + ve).

2.4. Equipments

Elemental analysis was carried out by using a Perkin-Elmer CHN 2400 and the metal contents were determined gravimetrically by ignition weighted samples in air atmosphere at 1,073 K to constant weight as the metal oxide forms and verified by complexometric analysis. The anion analysis was performed as follows: the complexes were dissolved in concentrated HNO_3, and the obtained samples diluted with water to 25 cm^3. The qualitative or quantitative analysis of Cl^- and SO_4 ions was performed by reactions with $AgNO_3$ and $BaCl_2$ solutions, respectively. IR spectra were recorded on a Bruker II FT-IR spectrophotometer (KBr discs) in the range from 4,000 to 400 cm^{-1}. ^{1}H-NMR and ^{13}CNMR spectra were recorded on a Varian Gemini 200 MHz spectrometer using DMSO-d^6 as solvent. The ESR spectra of powder Cu(II) complex at 300 k were recorded on a Bruker

EMX Spectrometer working in the x-band (9.78 MH) with 100 kHz modulation frequency, 1 mw microwave power and 4G modulation amplitude. The UV-vis spectra were performed in a DMSO solvent with concentration (1.0 $X10^{-3}$ M) and also in nujol mull for both free ciprofloxacin ligand and its complexes using a Jenway 6405 spectrophotometer with 1 cm quartz cells in the range of (800 to 200) nm. The effective magnetic moments were evaluated by applying $\mu_{eff} = 2.828\sqrt{x_M T}$, where X_M is the molar susceptibility corrected using Pascal's constants for the diamagnetism of all atoms in the ligand. Molar conductivities in DMSO at 10^{-3} mol dm^{-3} concentration were measured on a Jenway 4010 conductivity meter. The X-ray powder diffraction patterns of ciproH ligand and some of its complexes were recorded with a Rikagu diffractometer using Cu/Ka radiation. Scanning electron microscopy (SEM) images were taken in Joel JSM- 639OLA equipment, with an accelerating voltage of 20 KV. Thermogravimetry was measured (20-900 ^oC) on a Shimadzu TGA-50. The nitrogen flow and heating rate were 20 ml min^{-1} and 10 ^oC min^{-1}.

3. Results and Discussion

The isolated complexes are stable in air, have high melting points (> 300 ^oC), insoluble in water and common organic solvents but are soluble in DMF and DMSO. The conductivity measurements refer to a non conducting feature with Cu(II), VO(II) and Zn(II) complexes but a conducting feature with Pd(II), Pt(II) and Pt(IV) complexes through introducing 120, 110 and 105 $\Omega^{-1}cm^2mol^{-1}$values. The values may propose the presence of two anions inonically attached with the complex sphere. Attempts to propose the structures of the isolated complexes come from full investigation using the following studies starting with the elemental analysis (Table 1).

3.1. IR data and bonding mod

A comparative study on the IR complexes spectra with that of ciproH ligand displays the following information; the spectra of $[Cu(NO_3)_2(ciproH)_2]H_2O$, $[Pd(ciproH)_2]2Cl.H_2O$, $[Zn(NO_3)_2(ciproH)_2]2H_2O$, $[Pt(ciproH)_2]2Cl.H_2O$ and $[PtCl_2(ciproH)_2]2Cl.2H_2O$ complexes are relatively similar (Table 2), showing group of bands with different intensity at 2970 and 2820 cm^{-1}.

Table 1. Analytical data for ciproH ligand complexes

Compound Empirical formula	Color	Elemental analysis (%) Calcd. (Found)					
		Λ ($\Omega^{-1}cm^2 mol^{-1}$)	C	H	N	M	Cl
1) $[Cu(NO_3)_2(ciproH)_2]H_2O$	Green	20	47.03(47.21)	4.41(4.44)	12.90 (12.91)	7.32(7.27)	------
2) $[Pd(ciproH)_2]2Cl.H_2O$	yellow	120	47.59(47.58)	4.46(4.50)	9.79(9.78)	12.40(12.38)	……..
3) $[VO(ciproH)_2]2H_2O$	Green	35	58.19(58.10)	5.01(4.98)	11.01(11.11)	6.67(6.68)	-------
4) $[Zn(NO_3)_2(ciproH)_2]2H_2O$	White	33	45.98(45.89)	4.54(4.53)	12.62(12.61)	7.36 (7.35)	……
5) $[Pt(ciproH)_2]2Cl.H_2O$	Orange	110	43.14(43.12)	4.05(4.06)	8.88(8.83)	20.61 (20.60)	7.49(7.48)
6) $[PtCl_2(ciproH)_2]2Cl.2H_2O$	Yellow	105	39.43(39.44)	3.89(3.88)	8.11(8.11)	18.84(18.83)	13.69(13.68)

These bands can be assigned to the vibration of the quaternized nitrogen of the piperazinyl group which indicates the zwitterionic form of ciproH is involved in coordination to the metal ions [30] except $[VO(ciproH)_2]2H_2O$ complex displays a complete obscure for quaternized nitrogen bands. Such is verifying the coordination of cipro ions due to the presence of acetate anion in the reaction medium. New absorption bands appeared at ≈ 3420 and ≈ 1360 cm^{-1} in the spectra of all complexes and are attributed to lattice water molecules (υ and δOH, respectively). This suggestion was also supported by thermal analysis. The bands observed at 1775, 1720 and 1669 cm^{-1} in the spectrum of the free ciproH have been assigned to the stretching vibrations of the carboxylic (COOH) and the carbonyl (υC=O) groups, respectively [31–33]. The asymmetric stretching carboxylate bands appear at 1647, 1623, 1618, 1647 and 1642 cm^{-1} for the Cu(II), VO(II), Zn(II), Pt(II) and Pd(II), Pt(IV) complexes, respectively. The spectra of the complexes also show medium to strong intense bands near 1450 and 1380 cm^{-1}. These bands are most likely to the symmetric vibration of NO_3^- and ligated COO^- group. However, the peak observed at 1612 cm^{-1} in the IR spectrum of VO(II) complex indicates that assignment of this band to the asymmetric stretch υas(COO^-) of carboxyl group is doubtful [34]. The carboxylato group can act as a unidentate, bidentate or bridging ligand and distinction between these binding states can be made from the frequency separation [$\Delta\upsilon = \upsilon_{as}(COO^-) - \upsilon_s(COO^-)$] between the symmetric and asymmetric stretching of this group [34]. Unidentate carboxylato complexes exhibit Δυ values around 200 cm^{-1} and for bidentate or chelating carboxylato complexes Δυ is smaller than ionic value (Δυ <100 cm^{-1}); bridging complexes show Δυ around 150 cm^{-1}. The observed Δυ for the complexes are around 200 cm^{-1}, table 2, suggesting a unidentate interaction of the carboxylate group. The υ(CO) in the spectrum of ciproH is at 1630 cm^{-1} as a shoulder. In the spectra of complexes, the υ(CO) bands are slightly effected by the interaction with metal ions and appear at 1620, 1623, 1625, 1625, 1620 or 1625 $cm^{-1}$with Cu(II), VO(II), Zn(II), Pd(II), Pt(II) and Pt(IV), respectively. Similar behavior has been observed in several quinolone-metal ion complexes [33, 34]. The coordination of metal ions via carboxylate or carbonyl group is confirmed by the υ (M–O) bands nearly 550 cm^{-1} with each metal ion. Accordingly, the ciproH acts as a bidentate ligand through the oxygen atom of the carbonyl group and one from

carboxylate group. The infrared spectra of the prepared complexes display changes in the aromatic ring vibrations in comparison to the corresponding absorption bands of free ciproH.

Table 2. Assignments of the IR Spectral bands (cm^{-1}) of ciproH and its metal complexes

CiproH	Cu(II)	VO(II)	Pd(II)	Zn(II)	Pt(II)	Pt(IV)	Assignments
3369	3420	3400	3410	3420	3415	3420	v(N H) + vas(O H); H_2O
3290, 2985,2963,2919	3062, 2970, 2820, 2930	---	2982, 2966, 2924	3063,2968,2970, 2924	3030,2968,2926, 2820	2967, 2926, 2970	vs(O H); H_2O, v (NH_2+)
1775, 1720	1728	1710	1708	1707	1708	1731	v(C= O): (COOH)
1669,1630	1647,1620	1612,1623	1642,1625	1625	1647,1620	1642,1625	vas(COO−)+v(C=O)
1492,--	1466,1550	1485,--	1455,--	1468,1555	1454,--	1454,--	CH; deformation of CH_2; v_{as}(O=N) : NO_3^-
1333,-- 1248,1154	1380,1455 1232, 1161	1365 1222,1158	1366 1230,1163	1363,1420 1262,1198	1366 1229,1121	1368 1239,1194	vs(COO^-) + v_s(N- O): NO_3^-, δw(CH_2)
							v(C-C); v(C-O)
760,698	726,696	760	728	727,697	727	727	δb(COO–) + δ(NO_2): NO_3^-
-----	560,469	550	555	560,401	565	565	v(M–O) + v(M–N) ring deformation

3.2.^{1}HNMR and ^{13}CNMR spectra

The ^{1}HNMR spectra are further support the assignment of the coordination modes. The spectra of Zn(II) and Pt(IV) complexes were carried out in DMSO-d^6 solvent (Fig. 2, a and b). Upon investigation of the free ligand spectrum, the absence of a signal appeared at ≈11 ppm assigned to the carboxylic OH. This supports the major presence of zwitterionic structure. Signals for down shifted pyridine –CH…O as a singlet at δ =8.8 (s, 1H), aromatic F-C-CH= at 7.31 (1H), a signal at 5.33 (s, 1H, Ar CH), signals of piperazine at ≈ 3.84 (m, 8H), signal at 2.51 for $^{+}NH_2$ and signals of cyclopropan at 1.45 – 1.57(m, 5H). The spectrum $[Zn(NO_3)_2(ciproH)_2]$ $2H_2O$ complex confirms the coordination of cipro ligand in its zwitter ionic form. Due to the different chemical environments, a higher shift of pyridine CH supports the decomposition of intraligand H- bonding after the coordination of COO^-. A signal is recorded for the quaternized nitrogen (–$^{+}NH_2$) at δ= 2.50 ppm. The peak at δ= 3.55 ppm can be assigned as coming from the water molecules of hydration, which were not detected in the spectrum of the free cipro ligand. Peaks at δ= 7.28 and 7.26 ppm may be assigned to aromatic CHs. The Pt(IV) complex spectrum display peaks at δ= 9.5, 7.28-7.38, 3.52, 2.57, 2.2 and 1.2-1.8 ppm assigned to pyridine, F-C-CH(2H), piperazine, $^{+}NH_2$, H_2O and cyclopropane. The ^{13}CNMR spectra of ciproH ligand and its corresponding

Zn(II) and Pt(IV) complexes reveals some information about the mode of bonding as well as the geometry of compounds supporting the IR data. The signal observed with the free ligand at δ 170.31, 126.37–129.02, 74.31, 57.53- 66.75 and 27.6 – 41.42 ppm for pyridine C=O, benzene C=C, carboxylic, piprazine and cyclopropane, respectively. The absence of an observable shift of carbon signals in the spectra (Fig. 3,a; b) of the two complexes confirms the disappearance of any rearrangement with the ligand body during the complexation in between the aromatic carbon signals observed in the range δ =126.37–129.02 ppm are remaining almost in the same position. This is expected behavior with ciproH compound.

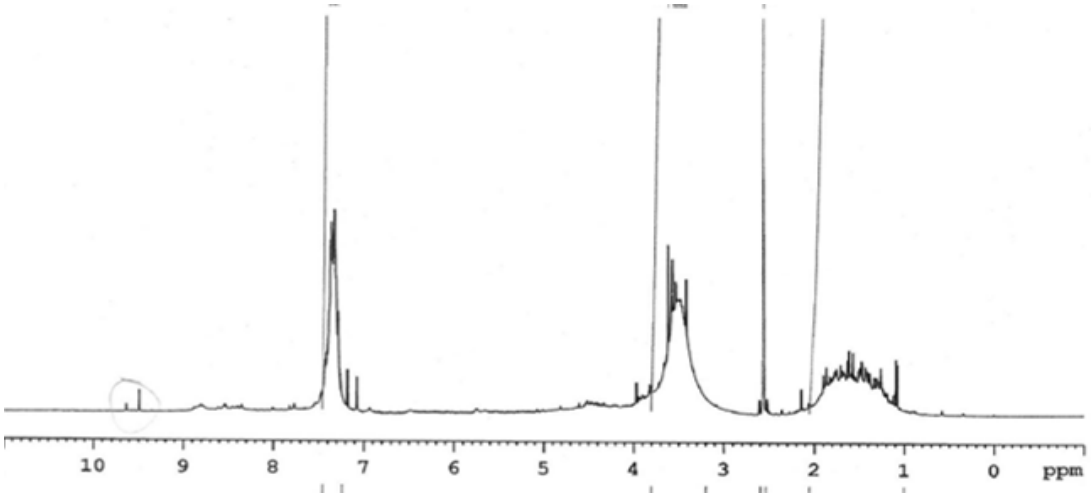

(a)

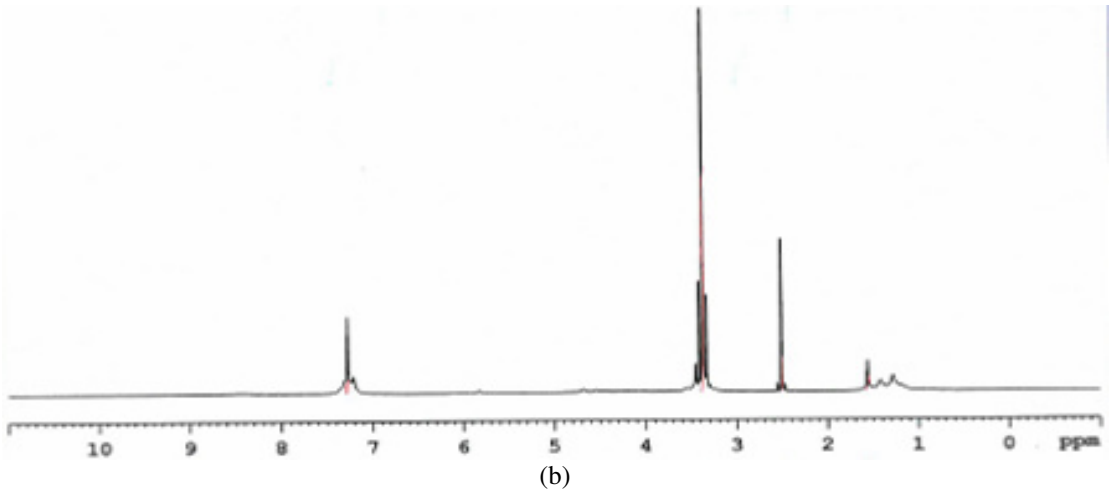

(b)

Figure 2. [1]HNMR Spectra of, a) Pt(IV) ; b) Zn(II) complexes

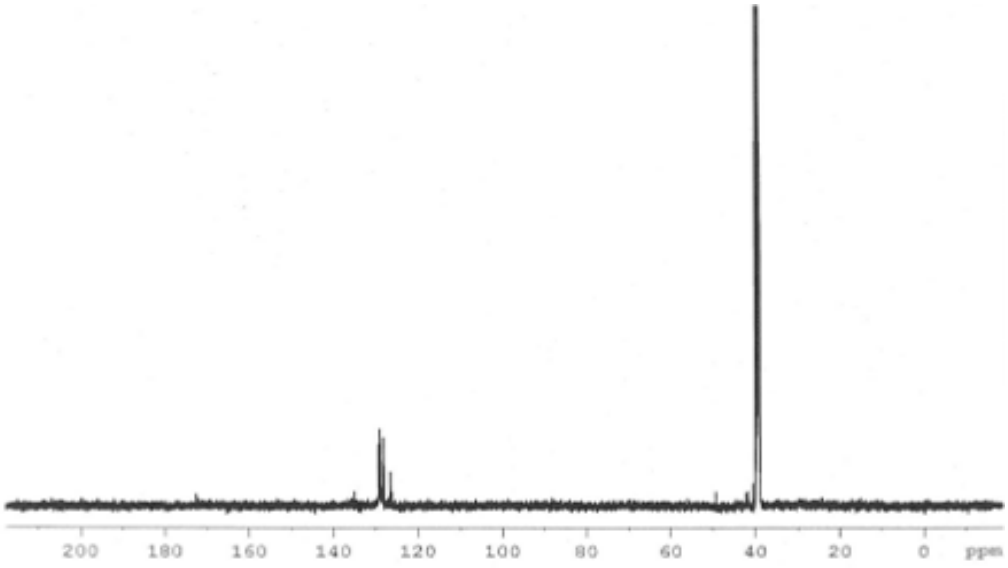

(a)

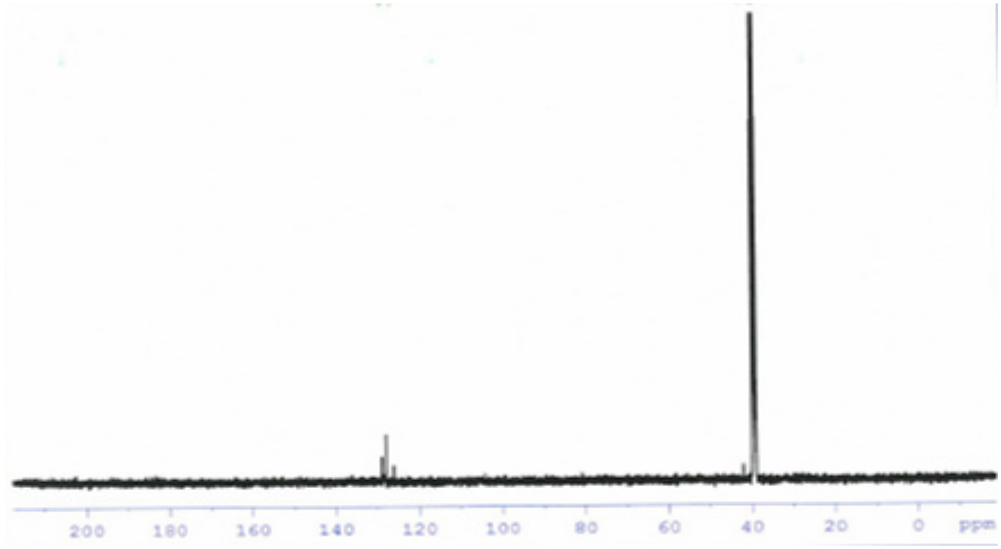

(b)

Figure 3. ^{13}CNMR Spectra of, a) Pt(IV) ; b) Zn(II) complexes

3.3. Electronic spectra and the magnetic measurements

Electronic spectra of the complexes and ciproH ligand were recorded in the 200–800 nm region in DMSO (Table 3). Two peaks appeared at 35,188 (band I) and 25,974 cm^{-1} (band II) in the ligand, attributed to n→π* and π →π* transitions (these transitions occur in case of unsaturated hydrocarbons which contain carbon atom attached with oxygen atom as in carboxylic and carbonyl groups). The electronic spectra of the complexes show that the two bands I and II in the electronic spectra are affected, obviously suggesting that the ligand has attached by a zwitterionic form. The copper(II) complex spectrum displays peak at 288 nm has hyperchromic effect to high absorbance than the ligand, and it should be assigned to carboxylic and carbonyl groups are involving in the complexation. An observable band at 14.881 cm^{-1} is assigned to $^{2}E_{g}\rightarrow{}^{2}T_{2g}$ transition, where that at 26,590 cm^{-1} may assign to O→Cu(II) [35] charge transfer. The normal magnetic moment (1.84 BM)value with the presence of orbital- orbital contribution obviously observed with O-bonded complexes [36]. The spectra of the Zn(II)

complex, the two bands are hypochromically affected obviously, suggesting that the ligand has attached by a zwitterionic form. The results clearly indicate that the ligand coordinates to the metal(II) ions via carboxylic and carbonyl groups, which is in accordance with the results of the FT-IR spectra. The VO(II) complex spectrum displays a well defined band observed at 11.890 cm^{-1} and assigned to $^2B_2 \rightarrow {}^2E(\nu_2)$ in a square-pyramidal configuration [37] by μ_{eff} = 1.71BM. It was proposed earlier [38] that the band at 980 cm^{-1} in the i.r. spectra of the VO^{2+} complexes is characteristic for the aforementioned structure. The present complex shows this band at 994 cm^{-1}. The color (green) may be considered as a further evidence for such postulation. The spectra of Pd and Pt(II) complexes display three d–d spin allowed corresponding to the transitions from the three lower lying 'd' orbital to the empty dx^2-y^2 orbital. The $^1A_{1g}$ ground state and the excited states corresponding to the above transitions are $^1A_{2g}$,$^1B_{1g}$ and $^1E_{1g}$ in order of increasing energy. These d–d transition bands in the regions, 19,801, 20,833; 23,509, 24,038 and 28,571, 27,624 cm^{-1} attributed to $^1A_{1g} \rightarrow {}^1A_{2g}$, $^1A_{1g} \rightarrow {}^1B_{1g}$ and $^1A_{1g} \rightarrow {}^1E_{1g}$ transitions, respectively. Three different orbital parameters Δ_1, Δ_2, Δ_3 have also been calculated by first using the correlation, for the Slater–Condon interelectronic repulsion parameters and subsequently the equations suggested by Gray and Ballhausen [39]. The υ_2/υ_1 were also calculated and are in close agreement with data reported earlier for the square planar geometry [40]. The electronic spectrum of Pt(IV) complex displays an observable $n \rightarrow \pi^*$ band at 28,230 cm^{-1}. The band at 22,680 cm^{-1} may be due to LMCT. Previous studies proved that the band in the region 25,000–26,040 cm^{-1} is assignable to $S(\sigma) \rightarrow Pt(IV)$ transition, the 20,600 cm^{-1} band is due to $S(\pi) \rightarrow Pt(II)$ transition [41,42] whereas the band at 21,790–24,750 is due to $O \rightarrow M(II)$ which is coincide with the study results. Table 3 shows the spectral bands of the investigated complexes. The spectra displayed charge transfer and spin allowed transitions correlated with an octahedral geometry [43].

Table 3. Magnetic moments (BM) and electronic spectra bands (cm^{-1}) of the complexes

Complex	μ_{eff} (BM)	d-d transition (cm^{-1})	Intraligand and charge transfer (cm^{-1})
1)	1.84	14.881	26,590 ; 28,571 ; 23,809
2)	0.0	----	19,801; 23,509; 28,571
3)	1.71	11.890	30,303 ; 23,256
4)	0.0	----	35,714; 30,303
5)	0.0	-----	20,833; 24,038 ; 27,624
6)	0.0	-----	28,230 ; 22,680

3.4. ESR spectrum of Cu(II) complex

The spin Hamiltonian parameters for Cu(II) complex (S=1/2, I = 3/2) were calculated (Table 4). The g tensor values can be used to derive the ground state. In square-planar or square pyramidal complexes, the unpaired electron lies in the d_{x2-y2} orbital giving $^2B_{1g}$ as the ground state with $g_{11}>g\perp>2.0023$, while giving $^2A_{1g}$ with $g\perp>g_{11}>2.0023$ if the unpaired electron lies in the d_z^2 orbital. From the observed values, $g_{11}(2.4) > g\perp (2.08) > 2.0023$ indicating that the copper site has a $d_x^2{}_{-y}^2$ ground state characteristic of a square pyramidal or octahedral geometry [44]. In axial symmetry, the g values are related by: $G = (g_{11}-2.0023)/(g\perp-2.0023) = 4$, if $G > 4$, the exchange interaction between copper(II) centers in the solid state is negligible, whereas when $G < 4$, a considerable exchange interaction is indicated. The G value of the complex (5.1) suggests the absence of exchange coupling between copper(II) centers in the solid state [45] supporting mononuclear structures. The tendency of A_{11} to decrease with increasing g_{11} is an index for the increase of the tetrahedral distortion in the coordination sphere of Cu [46]. In order to quantify the degree of distortion of the Cu(II) complexes, the f factor, g_{11}/A_{11}, (an empirical index of tetrahedral distortion) [47] was selected from the ESR spectrum. Although its value ranges between 105 and 135 for square planar complexes, the values can be much larger in the presence of a tetrahedral distorted structure. For the investigated complex, the g_{11}/A_{11} quotient is 171 cm^{-1} supporting the presence of significant dihedral angle distortion in the xy-plane and indicating a tetrahedral distortion from square-planar geometry. Molecular orbital coefficients, α^2(covalency of the in-plane σ-bonding) and β^2 (covalency of the in plane π-bonding) were calculated [48,49]. The α^2 value (0.75) is found lower than β^2 (0.88) indicating the ionic character of σ-bonding and π–bonding. The data agree with other reported values [50]. Superhyperfine structure is seen at higher field, supports an interaction of the nuclear spins of the C=O with the electron density on Cu(II). Furthermore, it has been reported that g_{11} is 2.4 for copper-oxygen bonds and 2.3 for copper-nitrogen bonds; in the studied complex, the g_{11} is 2.4 in conformity with oxygen metal bonds. Finally, the powder e.s.r (Fig.5) spectrum of the copper(II) complex as well as the g values agree with distorted octahedral complex [51

Table 4. ESR data of Cu (II) complex at room temperature

Complex	F	$g_{//}$	$g_{\perp}$	g_{iso}	$A_{//} \times 10^{-4}$ (cm^{-1})	G	α^2	β^2
171(1)		2.40	2.08	2.187	140.4	5.12	0.75	0.887

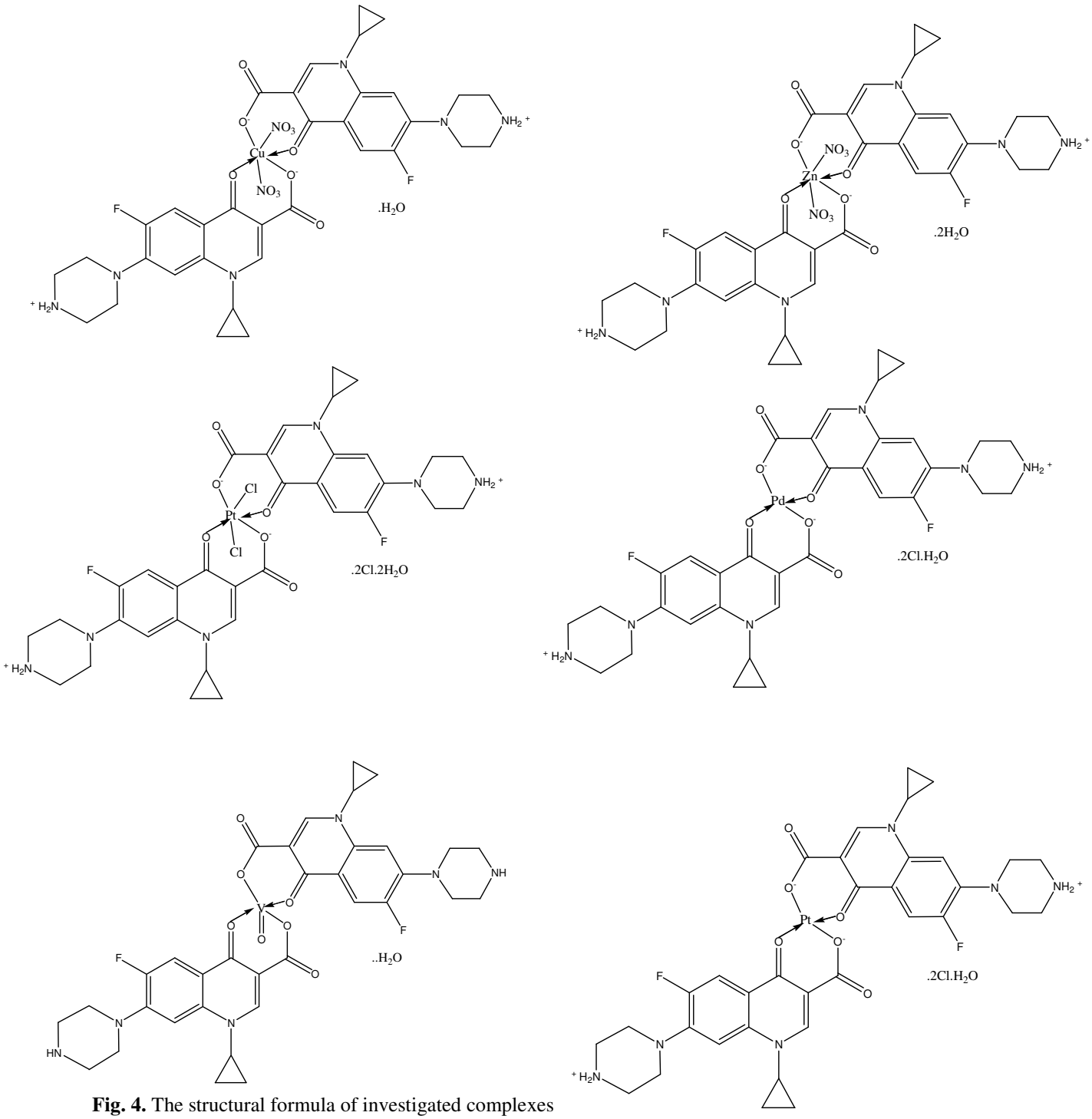

Fig. 4. The structural formula of investigated complexes

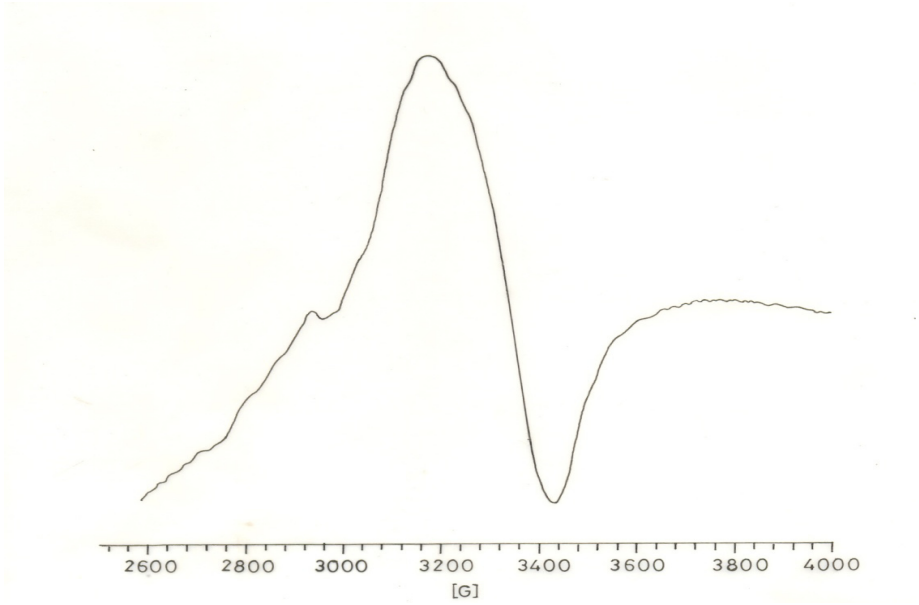

Figure 5. ESR Spectrum of Cu(II)- ciproH complex.

3.5. Thermogravimetric analysis

The decomposition stages, temperature ranges, proposed decomposition products as well as the calculated and found weight loss percentages of the complexes are presented in Table 5. In most investigated complexes, the first decomposition stage is attributed to the removal of hydrated water molecules. In $[Cu(NO_3)_2(ciproH)_2]H_2O$ complex, the TG and DTG curves show four decomposition stages started at 50˚C and ended at 620˚C. The complex reveals a lower thermal stability appeared by a sudden decomposition at 50 ^oC by 2.02 % weight loss corresponding to the elimination of hydrated H_2O molecule. The second and third endothermic decomposition stages started at 170 and 260˚C corresponding to the removal of HL and HL-O molecules by 38.16 and 36.52% weight losses, respectively. The final degradation stage started at 550˚C is translated to the removal of $2(NO_3)$ by 13.67% weight loss, lefts CuO at ≈ 620˚C as a residual part. The gradual degradation stages for $[Pd(ciproH)_2]2Cl.H_2O$ complex started at 35˚C and attributed to the expel of $H_2O + Cl_2$ by 10.28% weight loss. The second and third endothermic decomposition stages started at 180 and 390˚C corresponding to the stepwise removal of two ligand molecules by 38.61 and 38.52% weight losses, respectively, lefts Pd at ≈ 600˚C as a residual part. The gradual degradation stages representing in TG and DTG curves for $[VO(ciproH)_2]2H_2O$ complex started at 50˚C for the first degradation stage is attributed to the removal of $2H_2O$ by 4.62% weight loss. The second and third endothermic decomposition stages started at 120 and 360˚C corresponding to the stepwise removal of L and $C_{14}H_{17}FN_3$ molecules by 43.12 and 31.61% weight losses, respectively, lefts (VOC_3O_3H) at ≈ 510˚C as a residual part. The gradual degradation stages representing in TG and DTG curves (Fig. 6) for $[Zn(NO_3)_2(ciproH)_2]2H_2O$ complex started with sudden decomposition at low temperature 42˚C referring to the expel of two hydrated H_2O molecules by 4.25% weight loss. The second and third endothermic decomposition stages started at 175 and 405˚C corresponding to the stepwise removal of HL + HL-O and $2(NO_3)$ molecules by 72.62 and 13.50 % weight losses, respectively, lefts ZnO at ≈ 575˚C as a residual part. The gradual degradation stages representing in TG and DTG curves (Fig. 6) for $[Pt(ciproH)_2]2Cl.H_2O$ complex started with

sudden decomposition at 50˚C reflecting the thermal instability referring to crystall water molecule expelled with Cl_2 by 9.42% weight loss. The second and third endothermic decomposition stages started at 150 and 360˚C corresponding to the stepwise removal of HL and HL-O molecules by 35.10 and 33.24 % weight losses, respectively, lefts PtO at ≈ 590˚C as a residual part. The gradual degradation stages representing in TG and DTG curves (Fig. 6) for $[PtCl_2(ciproH)_2]2Cl.2H_2O$ complex started with sudden decomposition at 59 ˚C reflecting the thermal instability referring to the expel of $2H_2O$ + 2HL + Cl_2 molecules by 74.67 % weight loss. The second endothermic decomposition stage started at 470˚C corresponding to the removal of two chloride molecules by 7.19 % weight losses, lefts Pt atom at ≈ 600 ˚C as a residual part.

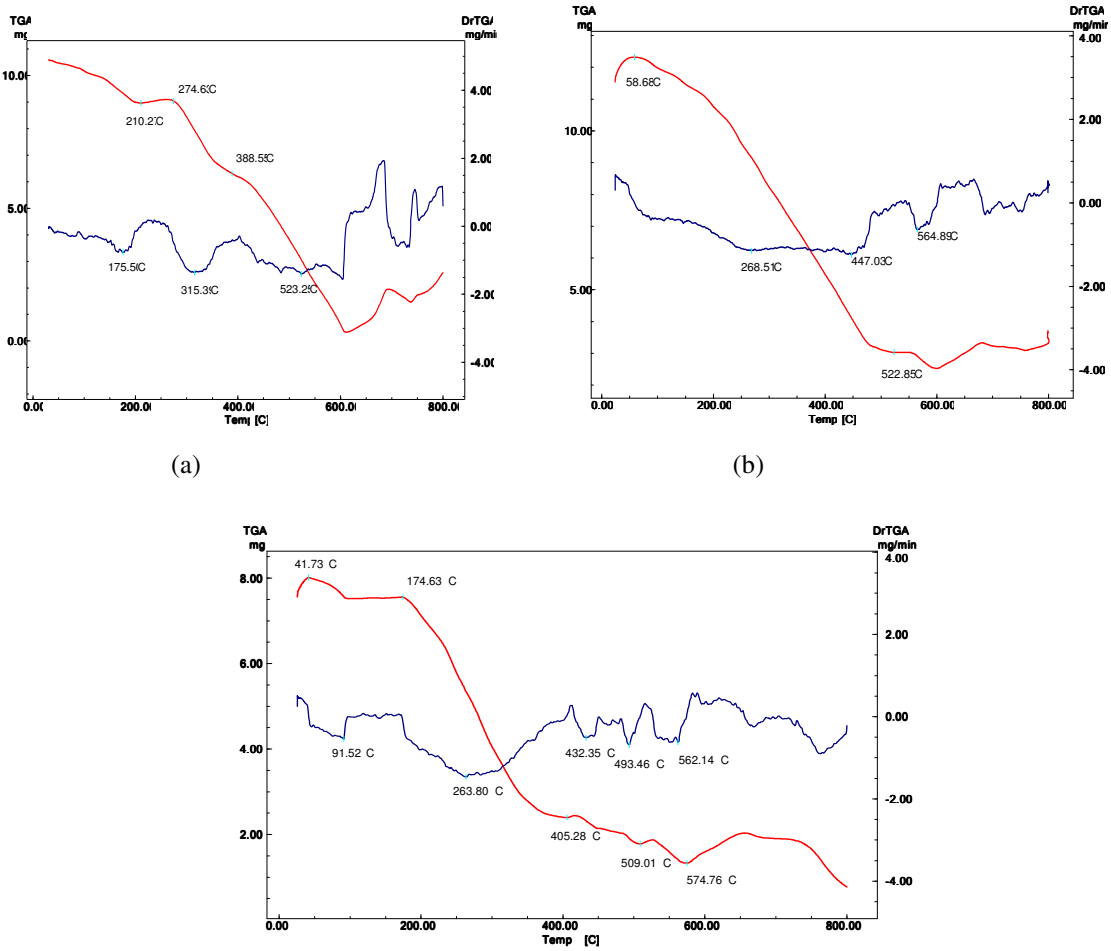

(a) (b)

(c)

Figure 6. The TG, DrTG curves of ; a) Pt(II), b) Pt(IV) and C) Zn(II) complexes

Table 5. Thermogravimetric analysis data of all investigated complexes

Complex	Steps	Temp. range (°C)	Decomposed assignments	Weight loss Found (Calcd. %)
(1)	1st	50 – 150	- H_2O	2.02 (2.07)
	2nd	170 – 260	-HL	38.16 (38.16)
	3rd	260 – 550	- HL-O	36.52 (36.32)
	4th	550 – 620	-2 (NO_3)	13.67 (14.28)
	residue		CuO	9.63 (9.16)
(2)	1st	35 – 180	-H_2O+ Cl_2	10.28(10.36)
	2nd	180– 390	- HL	38.61 (38.62)
	3rd	390 – 600	- HL	38.52 (38.62)
	residue		Pd	12.59 (12.40)
(3)	1st	50– 120	-2H_2O	4.62 (4.72)
	2nd	120 – 360	- L	43.21 (43.26)
	3rd	360 – 510	- $C_{14}H_{17}FN_3$	31.61 (32.25)
	residue		(VOC_3O_3H)	20.56 (19.77)
(4)	1st	42 – 175	-2H_2O	4.25 (4.06)
	2nd	175 – 405	- HL +HL-O	72.62 (72.82)
	3rd	405 – 575	- 2(NO_3)	13.50 (13.96)
	residue		ZnO	9.63 (9.16)
(5)	1st	50 – 150	- H_2O+ Cl_2	9.42 (9.39)
	2nd	150 – 360	- HL	35.10 (35.0)
	3rd	360 – 590	- HL-O	33.24 (33.31)
	residue		PtO	22.24 (22.29)
(6)	1st	59 – 470	- 2H_2O + 2HL + Cl_2	74.67(74.32)
	2nd	470 – 600	- 2 Cl_2	7.19 (6.85)
	residue		Pt	18.14 (18.84)

3.6. Kinetic studies

In order to assess the effect of metal ion on the thermal behavior of the complexes, the order n, and heat of activation E of suitable decomposition stages were determined from the TG and DTG (Table 6) curves. Three complexes are discussed as an example to emphasis on the degree of thermal stability during the degradation process. Several equations [52-59] have been proposed as means of analyzing TG curves and obtaining values for kinetic parameters. Many authors [52-55] have discussed the advantages of this method over the conventional isothermal method. The rate of decomposition process can be described as the product of two separate functions of temperature and conversion (2), using :

$$\frac{d\alpha}{dt} = k(T)\, f(\alpha) \qquad (1)$$

Where α is the fraction decomposed at time t, k(T) is the temperature dependant function and f(α) is the conversion function dependent on the mechanism of decomposition. The temperature dependent function k(T) is of Arrhenius type and can be considered as the rate constant k,

$$K = A\, e^{-E^*/RT} \qquad (2)$$

Where R is the gas constant in (J mol^{-1} k^{-1}) substituting equation (2) into equation (1) we get this equation :

$$\frac{d\alpha}{dT} = \left(\frac{A}{\varphi\, e^{-E^*/RT}}\right) f(\alpha) \qquad (3)$$

Where φ is the linear heating rate dT /dt. From the integration and approximation, this equation can be obtained in the following form :

$$\ln g(\alpha) = \frac{-E^*}{RT} + \ln\left[\frac{AR}{\varphi E^*}\right]$$

Where g(α) is a function of α dependant on the mechanism of the reaction. The integral on the right hand side is known as temperature integral and has no close for solution. So, several techniques have been used for the evaluation of temperature integral. Most commonly used methods for this purpose are the differential method of Freeman and Carroll [52] integral methods of Coat and Redfern [54], the approximation method of Horowitz and Metzger [59]. The kinetic parameters for the cipro complexes are evaluated using the following methods and the results are in good agreement with each others. The used methods are discussed briefly:

3.6.1 Coats – Redfern equation

The equation is a typical integral method, represented as :

$$\int_0^{\alpha} \frac{d\alpha}{(1-\alpha)^n} = \frac{A}{\varphi}\int_{T_1}^{T_2} \exp\left(\frac{-E^*}{RT}\right) dt$$

For convenience of integration the lower limit T_1 is usually taken as zero. This equation on integration gives :

$$\ln\left[\frac{-\ln(1-\alpha)}{T^2}\right] = \ln\left(\frac{AR}{\varphi E^*}\right) - \frac{E^*}{RT}$$

A plot of $\ln\left[\frac{-\ln(1-\alpha)}{T^2}\right]$ (LHS) against 1/T was drawn (Fig. 7). E* is the energy of activation in $Jmol^{-1}$ and calculated from the slop and A is (S^{-1}) from the intercept value. The entropy of activation ΔS* in (J $K^{-1}mol^{-1}$) was calculated by using the equation :

$$\Delta S^* = R \ln\left(\frac{Ah}{K_B T_s}\right) \qquad (4)$$

Where k_B is the Boltzmann constant, h is the Plank's constant and T_s is the DTG peak temperature [59]

3.6.2 Horowitz – Metzger equation

The authors derived the relation :

$$\ln\left[-\ln(1-\alpha)\right] = \frac{E}{RT_m}\Theta \qquad (5)$$

Where α, is the fraction of the sample decomposed at time t and $\Theta = T - T_m$.

A plot of $\ln\left[-\ln(1-\alpha)\right]$ against Θ (Fig. 7) was found to be linear, from the slope of which E, was calculated and Z can be deduced from the relation :

$$Z = \frac{E\varphi}{RT_m^2}\exp\left(\frac{E}{RT_m}\right) \quad (6)$$

Where φ is the linear heating rate, the order of reaction, n, can be calculated from the relation :

$$n = 33.64758 - 182.295\alpha_m + 435.9073\alpha_m^2 - 551.157\alpha_m^3 + 357.3703\alpha_m^4 - 93.4828\alpha_m^5 \quad (7)$$

Where α_m is the fraction of the substance decomposed at T_m .

The entropy of activation, ΔS*, was calculated from equation (4). The enthalpy of activation ΔH*, and Gibbs free energy, ΔG*, were calculated from; ΔH* = E* -RT and ΔG* = ΔH* - TΔS*, respectively. The data tabulated reveals the following observations: (i) the activation energy E, increases somewhat through the degradation steps revealing the high stability of the remaining part suggesting a high stability of complexes characterized by their covalence, (ii) the negative ΔS* values, indicates the activated fragment has ordered structures (iii) the positive ΔH* reflects the endothermic decomposition process, (iv) the positive ΔG* singe reveals that the free energy of the final residue is higher than that of the initial compound, and the decomposition stages are non – spontaneous. This results from increasing TΔS* clearly from one step to another which override the values of ΔH* reflecting that the rate of removal of the subsequent species will be lower than that of the precedent one [60].

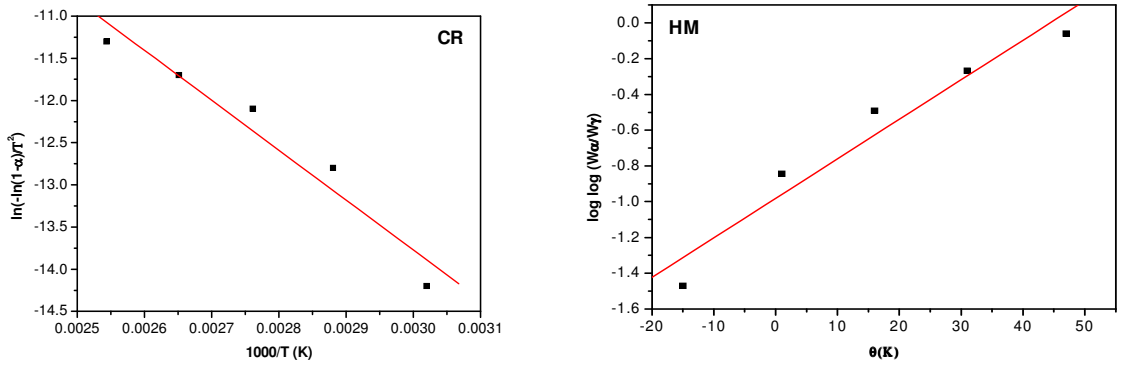

(a)

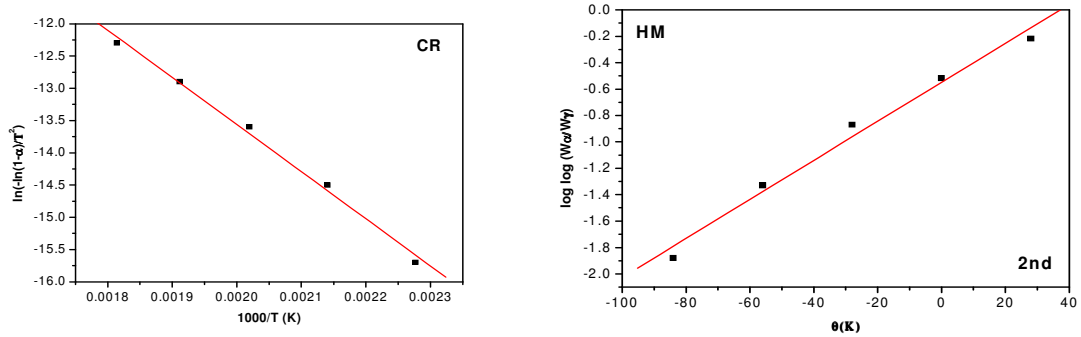

(b)

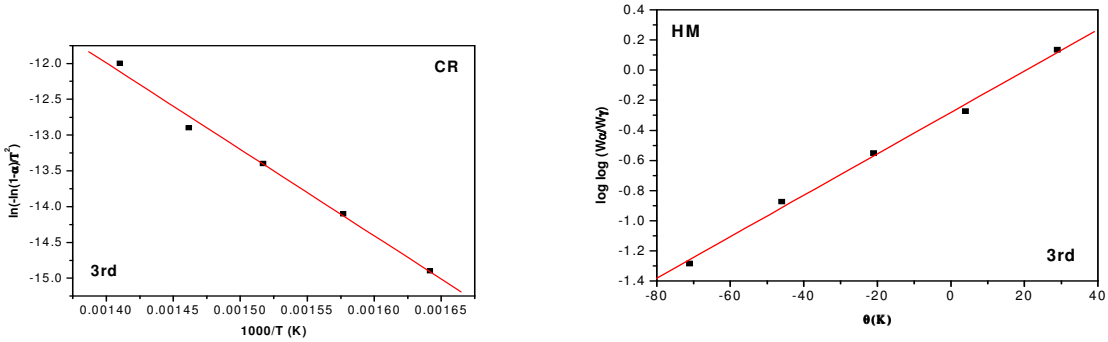

(c)

Figure 7.Coats Redfern (CR) and Horowitz–Metzger (HM) plots of the ligand and it's,
a) Pt(II), b) Pt(IV) and C) Zn(II) complexes

3.7. Scanning electron micrography

The morphology and particle size of some investigated complexes were obtained from scanning electron micrography (SEM). Cu(II) and Pt(II) complexes have the same shapes (Fig. 8 a,b). It is clear that these complexes have uniform matrix and homogeneity. The SEM of the two complexes displays the same sized slightly crystalline particles (5 µm) and ships. The surface morphology micrograph reveals the well sintered nature of the complexes. Clear large grains are obtained with agglomerates for all complexes. The distribution of the grain size is homogeneous except for Pt(IV) complex (Fig. 8c), The complex particles are fused to each other's which prohibit to justify about crystallinity. Such reflects the amorphous presence coincide with X-ray diffraction pattern.

\

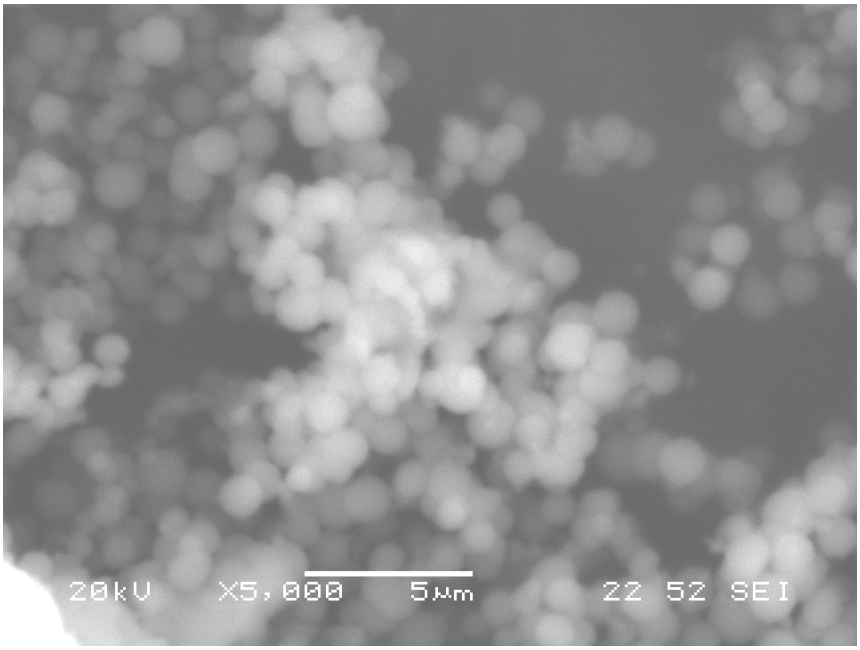

(a)

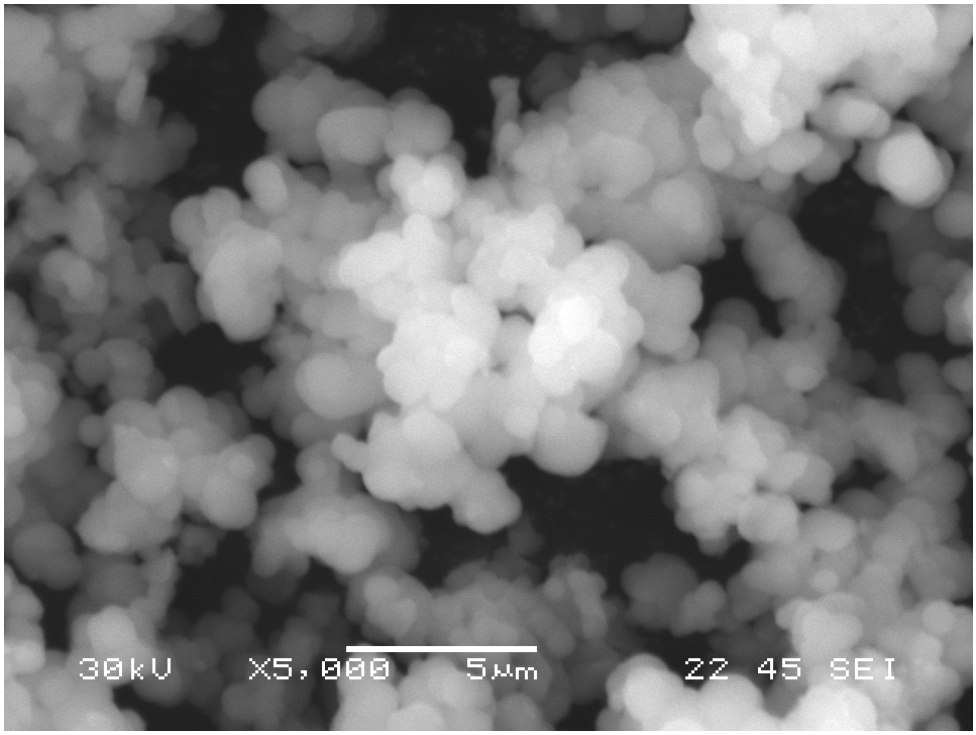

(b)

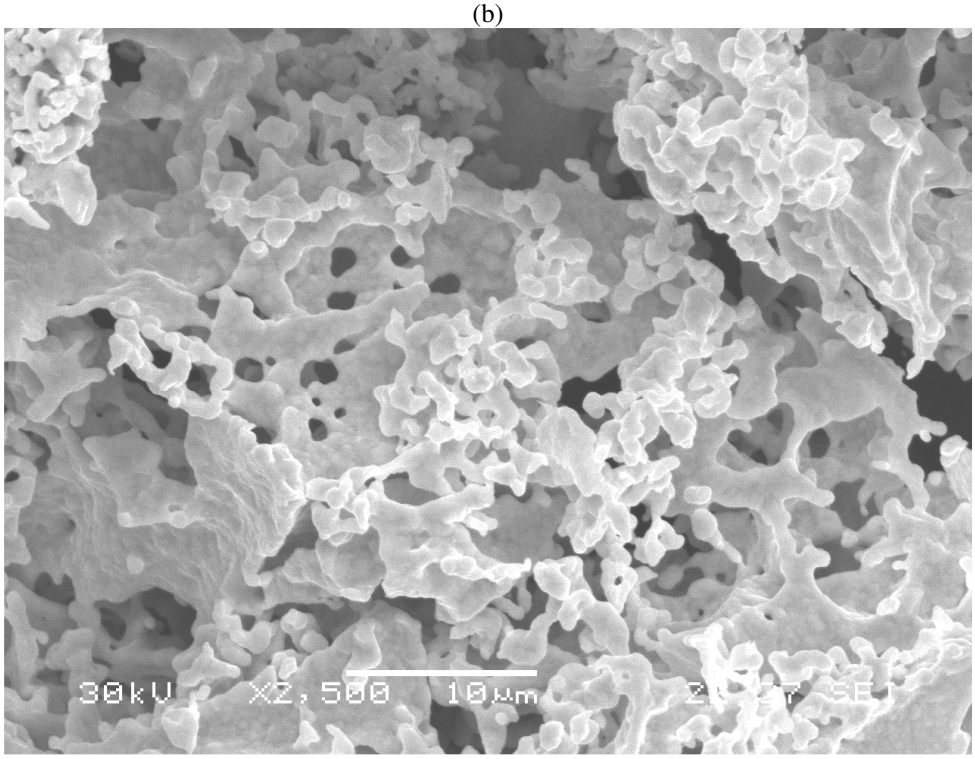

(c)

Figure 8. SEM images of , a) Cu(II),b) Pt(II) and C) Pt(IV) complexes

Table 6. Kinetic parameters using the Coats – Red fern (CR) and Horowitz – Metzger (HM) operated for the complexes.

Compounds	DTG_{max}	steps	Thermodynamic parameters		
			CR	HM	Units
Pd(II) complex	195°C	1st	E	4.90E+04	5.08E+04	J mol^{-1}
			A	7.90E+04	5.72E+05	s^{-1}
			ΔS	-1.54E+02	-1.38E+02	$Jmol^{-1}K^{-1}$
			ΔH	4.65E+04	4.80E+04	J mol^{-1}
			ΔG	9.90E+04	9.55E+04	J mol^{-1}
			r	0.9720	0.9712	
Zn(II) complex	366 °C	2nd	E	1.03E+05	1.25E+05	
			A	4.20E+05	1.85E+07	
			ΔS	-1.46E+02	-1.15E+02	
			ΔH	9.50E+04	1.22E+05	
			ΔG	1.94E+05	1.92E+05	
			r	0.9956	0.9975	
Pt(IV)complex	413 °C	2nd	E	6.10E+04	7.77E+04	
			A	5.30E+03	4.60E+05	
			ΔS	-1.79E+02	-1.43E+02	
			ΔH	5.66E+04	7.35E+04	
			ΔG	1.53E+05	1.44E+05	
			r	0.9973	0.9925	

r = correlation coefficient of the linear plot.

3.8. X – ray powder diffraction of the ligands and their complexes

X – ray powder diffraction patterns in the Θ °<2Θ < 60 °of ciproH ligand (Fig. 9) and its metal complexes were carried out in order to give an insight about the lattice dynamics of these compounds. The x – ray powder diffraction obtained reflects a shadow on the fact that each solid represents a definite compound of a definite structure which is not contaminated with starting materials. The pattern appearance of ciproH ligand is proposed a nanocrystalline nature, which identified through observing smooth peaks, but all investigated complexes are displaying less intense broad peaks for amorphous nature (Pd(II) as example). The somewhat difference observed with the appearance of Cu(II) and Pt(II) complexes with SEM may refer to the slight crystallinity of the surface particals.

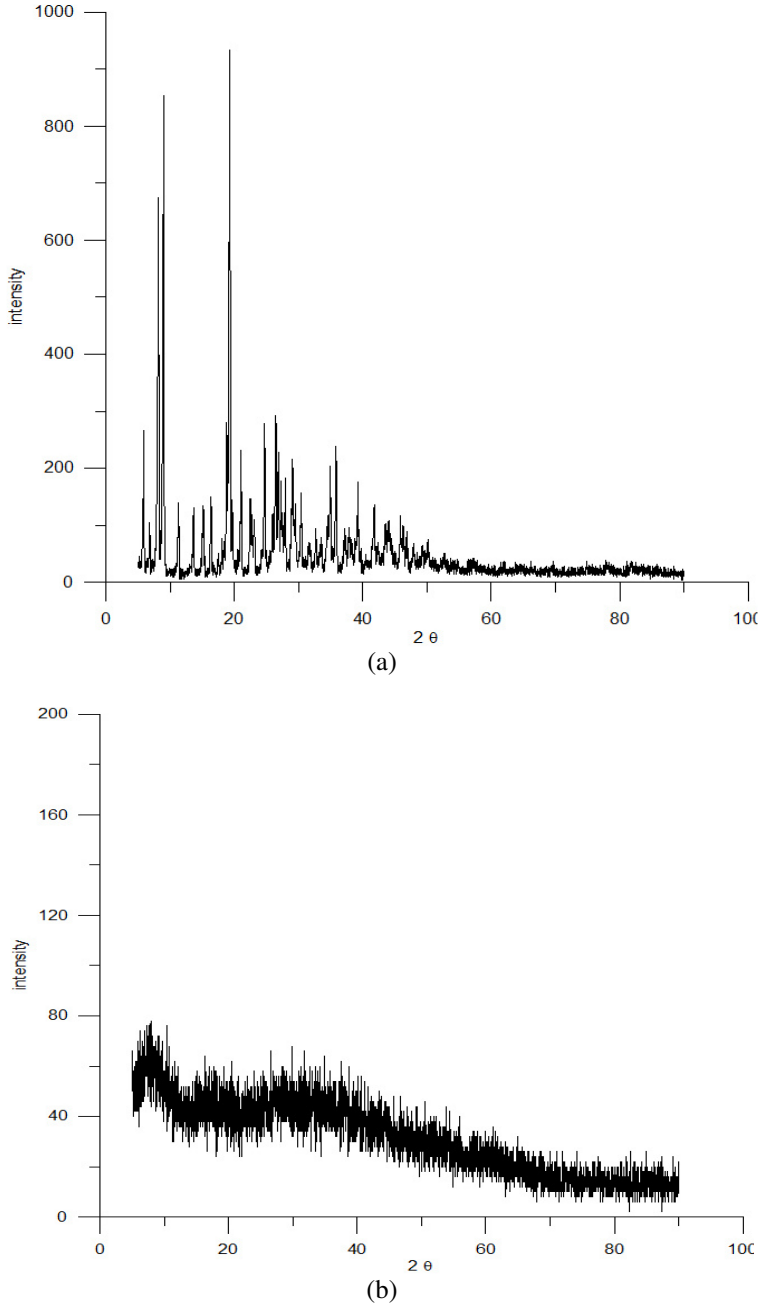

Figure 9. The X- ray Diffraction patter of, a) free ligand and b) Pd(II) complex

3.9. Molecular modeling of complexes

An attempt to gain a better insight on the molecular structure of the ligand and its complexes geometry optimization and conformational analysis has been performed by the use of MM^{+} force field implementing software Chem Office Ultra- 7. Molecular modeling had been successfully used to detect three dimensional arrangements of atoms in complexes (Fig. 10). The total internal energy for all complexes were calculated and the following arrangements starting with the most stable one; Zn(II)= 92.4942, Cu(II) = 94.2101, VO = 94.709,

Pd(II) = 123.2881,Pt(IV) = 124.2628, Pt(II) = 126.4390 kcal/mol. The stability proposed based on the theoritical calculation is going in a parrallel with the invers relation towards the metal ion size.

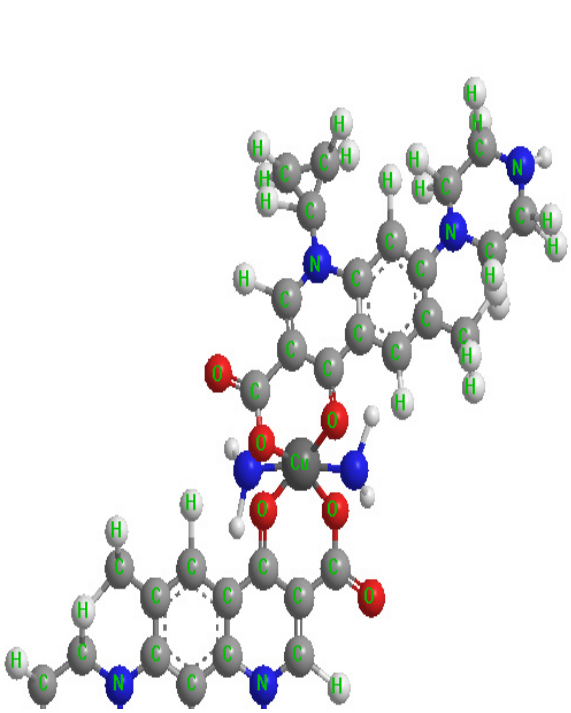

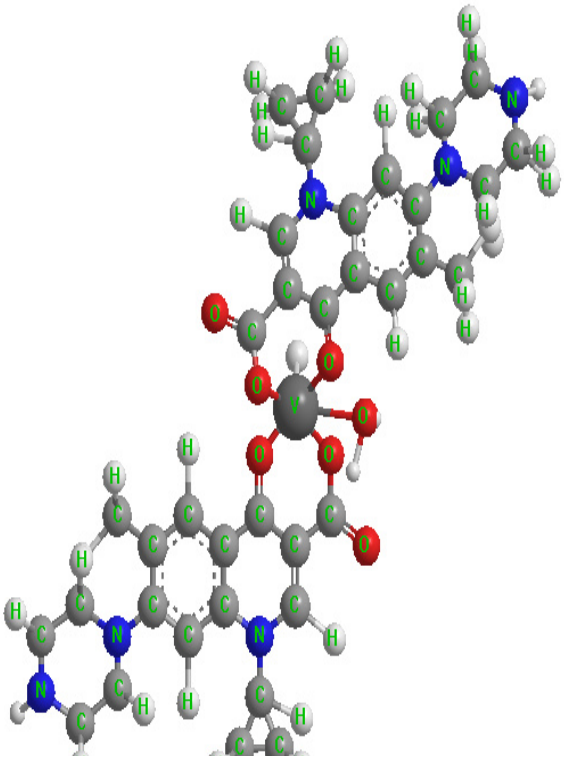

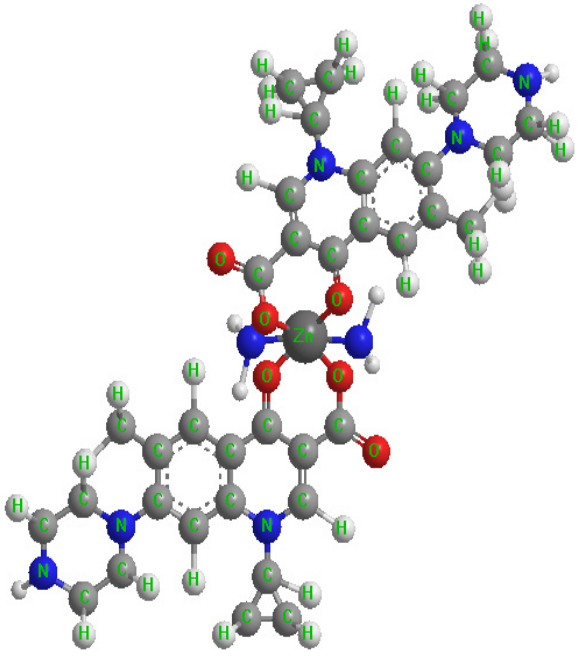

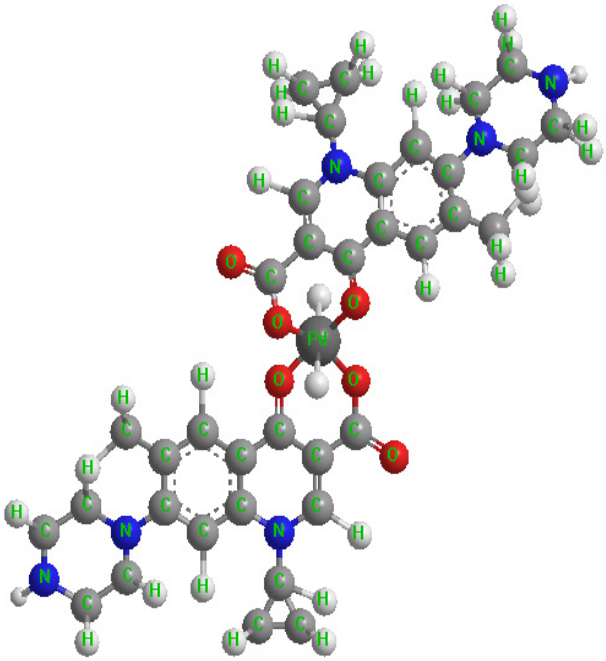

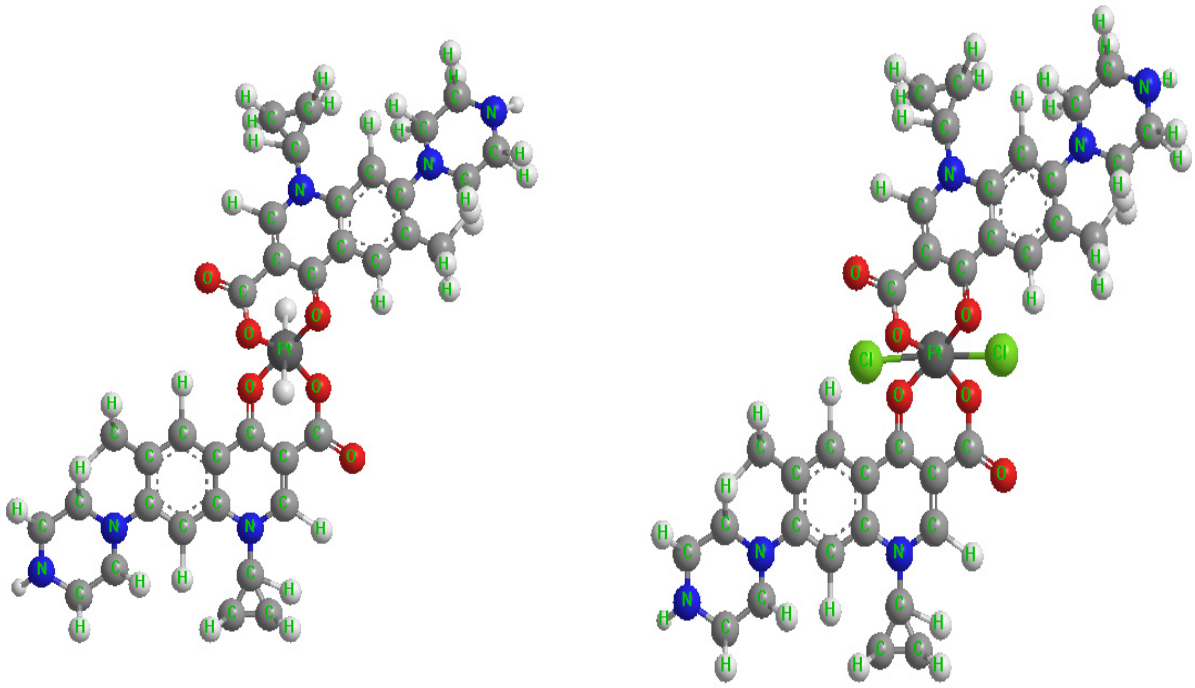

Fig. 10. The molecular modeling drown theoretically for investigated complexes

3.10. Antimicrobial studies

Biological studies were observed in term anti-microbial activities of target compounds against gram-positive (Bacillus sp) and gram-negative (Klebsiella sp. and Proteus sp). Results from the agar disk diffusion tests for anti-microbial activities of target compounds are presented in Table 7 and an explanation graph in figure 11. Generally speaking the antimicrobial activities were scored according to the Clinical Laboratory and Standards Institute (CLSI) and classified into three categories: R: resistant microbe (the diameter of the zone of inhibition equal 1.4 Cm or less), I: intermediate sensitive microbe(the diameter of the zone of inhibition ranges from 1.5-1.7Cm) and S: sensitive microbe to the tested agent (the diameter of the zone of inhibition is more than 1. 8 Cm). From the data presented in Table 7 it was found that Bacillus sp., Proteus and klebsiella are sensitive to the most of complexes. Some complexes showed bacteriostatic activity, meaning the complex initially suppressed the growth of the target microbe in the immediate contact vicinity for about 24 hours, then the complex degrades fast and the inhibited microbes resume growth in the same vicinity. The most reasons for the inhibition action of tested compounds may be due to their interactions with critical intracellular sites causing the death of cells. The variety of anti-microbial activities of tested compounds may due to different degree of tested compounds penetration through cell membrane structure of target organism. In conclusion, The effective antibiotic behavior was shined with the free ciproH ligand which is considered a normal behavior, but the priority of Zn, Pt(II) and Pt(IV) complexes in comparing with the free ligand is considered new. Such results may offer new antibiotic drugs serve distinguish than the introduced antibiotic (ciproH) drug in the medicinal field.

Table 7. The values of zone inhibition of bacteria for the ligand and its metal complexes.

Compound	Zone of inhibition (mm)		
	Bacillus Sp. Gram (+)	Klebsiella sp. Gram (-)	Proteus sp.
ciproH	2.0S	1.4I	2.0S
Cu(II)	2.0S	1.2R	1.8S
Pt(II)	2.2S	2.1S	2.3S
Pd(II)	1.4R	1.6I	1.0R
VO(II)	1.6I	1.3R	0.0
Pt(IV)	2.0S	2.0S	1.6I
Zn(II)	2.5S	2.0S	2.8S

R : resistant ; I : intermediate ; S: sensitive

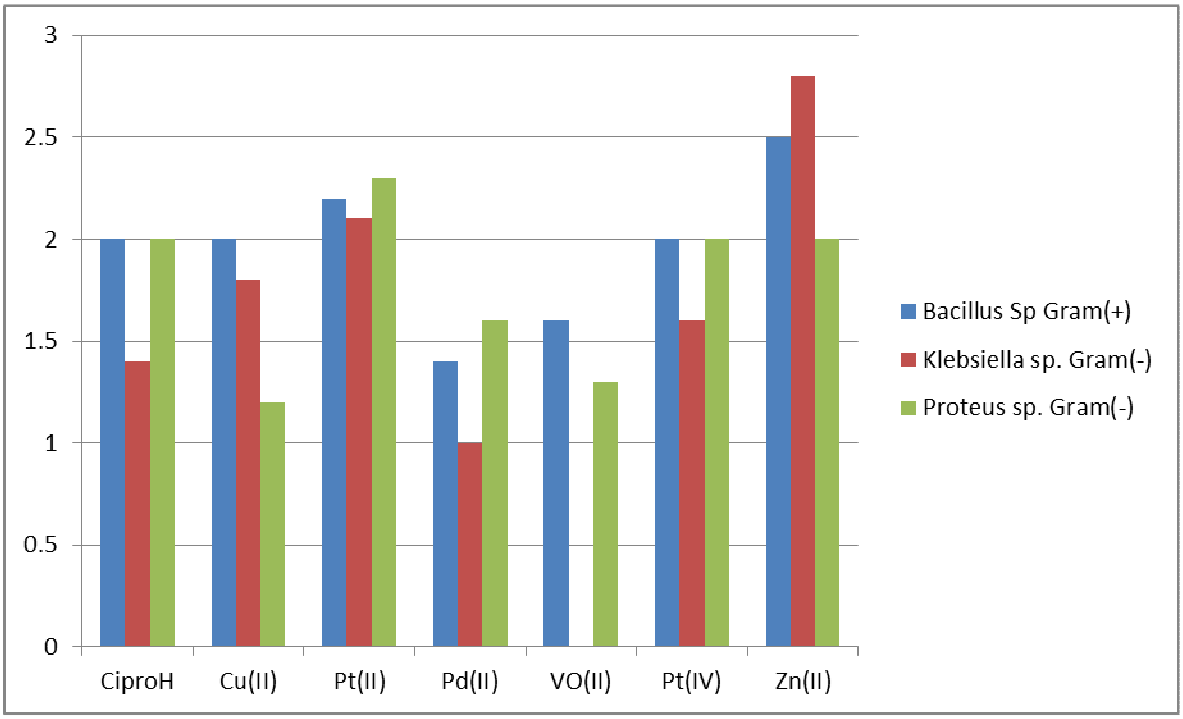

Figure 11. The graphical relation of diameter inhibition zone with the tested compounds for biological investigation.

References

[1] S.A. David, K.A. Balasubramanian, V.I. Mathan, P. Balaram, Biochim. Biophys. Acta 1165 (1992) 145.
[2] (a) J.W. Lown, Chem. Soc. Rev. 22 (1993) 65;
(b) D.R. Phillips, C. Cullinane, H. Trist, R.J. White, In vitro transcription analysis of the sequence specificity of reversible and irreversible complexes of adriamycin with DNA, in: B. Pullman, J. Jortner (Eds.), Molecular Basis of Specificity in nucleic acid–drug interactions, Springer, Berlin, 1990, pp. 137.
[3] J.F. Hinton, R.E. Koeppe, Biol. Syst. 19 (1985) 173.
[4] M.W. Parker, F. Pattus, A.D. Tucher, D. Tsernoglou, Nature 337 (1989) 93.
[5] (a) T. Oka, K. Hashizume, H. Fujita, J. Antibiot. 33 (1980) 1357; (b) J.M. Frere, J.M. Ghuysen, P.E. Reynolds, R. Moreno, Biochem. J. 143 (1974) 241.
[6] (a) H. Umezawa, M. Ishizuka, H. Suda, M. Hamadam, T. Takeuchi, J. Antibiot. 29(1976) 97; (b) H. Umezawa, M. Ishizuka, T. Aoyagi, T. Takeuchi, J. Antibiot. 29 (1976) 857.
[7] T. Osada, S. Ikegami, K. Takiguchi-Hayashi, Y. Yamazaki, Y. Katoh-Fukui, T. Higashinakagawa, Y. Sakaki, T. Takeuchi, J. Neurosci. 19 (1999) 6068.

[8] A. Zaki, E.C. Schreiber, I. Weliky, J.R. Knill, J.A. Hubsher, J. Clin. Pharmacol. 14(1974) 118.
[9] J. Klastersky, D. Daneau, D. Weerts, Chemotherapy 18 (1973) 191.
[10] J.R. Anacona, J. Coord. Chem. 54 (2001) 355.
[11] M.J. Lozano, J. Borrás, J. Inorg. Biochem. 31 (1987) 187.
[12] A. Zhao, C.E. Carraher, G. Barone, C. Pellerito, M. Scopelliti, L. Pellerito, Mater. Sci. Eng. 93 (2005) 414.
[13] M.S. Iqbal, A.R. Ahmad, M. Sabir, S.M. Asad, J. Pharm. Pharmacol. 51 (1999) 371.
[14] J.R.J. Sorenson, J. Med. Chem. 19 (1976) 135.
[15] D.H. Brown, W.E. Smith, J.W. Teape, A.J. Lewis, J. Med. Chem. 23 (1980) 729.
[16] D.R. Williams, The Metals of Life, Van Nostrand Reinhold, London, 1971.
[17] M. Ruiz, L. Perelló, R. Ortiz, A. Castiñeiras, C. Maichle-Mössmer, E. Cantón, J. Inorg. Biochem. 59 (1995) 801.
[18] S.E. Castillo-Blum, N. Barba-Behrens, Coord. Chem. Rev. 196 (2000) 3.
[19] I. Turel, I. Leban, N. Bukovec, J. Inorg. Biochem. 66 (1997) 241.
[20] I. Turel, L. Goli, P. Bukovec, M. Gubina, J. Inorg. Biochem. 71 (1998) 53.
[21] P. Yang, J.B. Li, Y.N. Tian, K.B. Yu, Chin. Chem. Lett. 10 (1999) 879.
[22] G. Wu, G. Wang, X. Fu, L. Zhu, Molecules 8 (2) (2003) 287.
[23] I. Turel, I. Leban, G. Klintschar, N. Bukovec, S. Zalar, J. Inorg. Biochem. 66 (1997)77.
[24] I. Turel, K. Gruber, I. Leban, N. Bukovec, J. Inorg. Biochem. 61 (1996) 197.
[25] I. Turel, I. Leban, M. Zupancic, N. Bukovec, K. Gruber, Acta Crystallogr. Sec C: Cryst. Struct. Commun. 52 (1996) 2443.
[26] Z.-F. Chen, R.-G. Xiong, J.-L. Zuo, Z. Guo, X.-Z. You, H.-K. Fun, J. Chem. Soc. Dalton Trans. (2000) 4013.
[27] J. Al-Mustafa, Acta Chim. Slov. 49 (2002) 457.
[28] M. Ruíz, L. Perelló, J. Server-Carrió, R. Ortiz, S. García-Granda, M.R. Díaz, E. Cantón, J. Inorg. Biochem. 69 (1998) 231.
[29] Gupta, R.; Saxena, R. K.; Chaturvedi, P.; Virdi, J. S. Chitinase , J. Appl. Bacteriol. 78(1995) 378.
[30] R.M. Silverstein, G.C. Bassler, T.C. Morril. Spectroscopic Identification of Organic Compounds, 5th Edn, Wiley, New York, 1991.
[31] I. Turel, I. Leban, G. Klintschar, N. Bukovec, S. Zalar. J. Inorg. Biochem., 66(1997) 77.
[32] I. Turel, I. Leban, N. Bukovec. J. Inorg. Biochem., 66(1997) 241
[33] F. Gao, P. Yang, J. Xie, H. Wang. J. Inorg. Biochem., 60(1995) 61 .
[34] Z.F. Chen, B.Q. Li, Y.R. Xie, R.G. Xiong, X.Z. You, X.L. Feng. Inorg. Chem. Commun., 4(2001) 346 .
[35] E. Franco, E. Lopez- Trorres, M. A. Mendiola, M. T. Sevilla, Polyhedron, 19 (2000)441

[36] E.W. Ainscough, A. M. Brodie , J. D. Ranford and J. M. Waters, J. Chem. Soc. Dalton, Trans.,1251(1997)

[37]N. M. El-Metwally, I. M. Gabr and A.A. El-Asmy, Transition Met. Chem. **1**(2006) 71

[38]N.M. El-Metwally, R.M. El-Shzaly, I.M. Gabr, A.A. El-Asmy, Spectrochim. Acta, 61(2004) 1113

[39] H.B. Gray, C.J. Ballhausen, J. Am. Chem. Soc. 85 (1963) 260.
[40] M.K. Biyala, K. Sharma, M. Swami, N. Fahmi, R.V. Singh, Trans. Met. Chem. 33 (2008) 377.
[41] A.B.P. Lever, Inorganic Electronic Spectroscopy, Elsevier, Amsterdam,1986.
[42] J.P. Jasinski, J.R. Bianchani, J. Cueva, F.A. El-Saied, A.A. El-Asmy, D.X. West, Z. Anorg, Allg. Chem. 629 (2003) 202.
[43] G. Ponticelli, A. Spanu, M.T. Cocco, V. Onnis, Transition Met. Chem. 24(1999) 370.
[44] (a) G. Speie, J. Csihony, A.M. Whalen and C.G. Pipont, Inorg. Chem., 35(1996) 3519 ; (b) M. Ruf, B. Noll, M. Grone, G.T. Yee and C.G. Piepont, ibid. 36, 4860.

[45] a. B.J. Hathaway and D.E. Billing, Coord. Chem. Rev., 5 (1970)143.b. B.J. Hathaway, Struct. Bond. (Berlin), 57(1984) 551.

[46] a,. J.A. Wellman and F.B. Hulsbergen, J. Inorg. Nucl. Chem., 40(1978) 143,b,. U. Sagakuchi, A.W. Addison, J. Chem. Soc. Dalton Trans., 660 (1979).

[47] H. Yokoi and A.W. Addison, Inorg. Chem., 16 (1977)1341.

[48] K. Jayasubramanian, S.A. Samath, S. Thambidurai, R. Murugesan and S.K. Ramalingam, Transition Met. Chem., 20(1995) 76

[49] V.S.X. Anthonisamy, R. Anantharam and R. Murugesan, Spectrochimica Acta, 55A(1999) 135.

[50] R.K. Ray and G.R. Kauffman, Inorg. Chem. Acta, 173(1990) 207)

[51] R.C. Maurya and S. Rajput, J. Molecular Structure, 687(2004) 35

[52] E. S. Freeman, B. Carroll, J. Phys.Chem.62 (1958) 394.
[53] J. Sestak, V. Satava, W. W. Wendlandt, Thermochim. Acta, 7(1973) 333.
[54] A. W. Coats, J. P. Redfern, Nature 201(1964) 68.
[55] T. Ozawa, Bull. Chem. Sot. Jpn. 38 (1965)1881.
[56] W. W. Wendlandt, " Thermal Methods of Analysis", Wiley, New York, 1974
[57] J. H. F. Flynn, L. A. Wall, J. Res. Natl. Bur. Stand. A 70 (1996) 487.
[58] P. Kofstad, Nature 179 (1957)1362.
[59] H. W. Horowitz, G. MJetzger, Anal. Chem. 35(1963)1464.
[60] S. S. Kandil, G. B. El- Hefnawy, E. A. Baker, Thermochim. Acta 414 (2004)105.

The IISTE is a pioneer in the Open-Access hosting service and academic event management. The aim of the firm is Accelerating Global Knowledge Sharing.

More information about the firm can be found on the homepage:
http://www.iiste.org

CALL FOR JOURNAL PAPERS

There are more than 30 peer-reviewed academic journals hosted under the hosting platform.

Prospective authors of journals can find the submission instruction on the following page: http://www.iiste.org/journals/ All the journals articles are available online to the readers all over the world without financial, legal, or technical barriers other than those inseparable from gaining access to the internet itself. Paper version of the journals is also available upon request of readers and authors.

MORE RESOURCES

Book publication information: http://www.iiste.org/book/

Recent conferences: http://www.iiste.org/conference/

IISTE Knowledge Sharing Partners

EBSCO, Index Copernicus, Ulrich's Periodicals Directory, JournalTOCS, PKP Open Archives Harvester, Bielefeld Academic Search Engine, Elektronische Zeitschriftenbibliothek EZB, Open J-Gate, OCLC WorldCat, Universe Digtial Library , NewJour, Google Scholar